Atomistic simulation of electro-osmosis in a nanometer-scale channel

By J. B. Freund†

An atomistic simulation of an electro-osmostic flow in a 50Å wide channel is performed to examine models for such flows and study its physical details. The working fluid considered is a 1.1M mean concentration solution of Cl^- in water. For simplicity and computational efficiency, only negatively charged ions are in the solution. The water is modeled by the SPC/E potential, and the Cl^- are modeled as point charges plus an established Lennard-Jones potential. The channel walls are fixed lattices of positively charged Lennard-Jones atoms. An aperiodic implementation of the P^3M algorithm is used to compute electrostatic interactions. The distribution of Cl^- adjacent to the charged walls differs somewhat from theoretical predictions that assume infinitesimal ions and constant electric permittivity, and this second assumption is called into question because it is found that the waters near the wall are preferentially oriented by the local electric field, which will alter their dielectric properties. When an electric field is applied parallel to the channel walls, a velocity profile develops that is consistent with a monolayer thick Stern layer fixed to the channel walls.

1. Introduction

Where an electrolyte fluid contacts a solid surface, it is common that the surface becomes charged with counter ions preferentially distributed above it in a thin layer (see Fig. 1). This layer of fluid that has a net charge is called the electric double layer, and the ion density within it is typically modeled by a Boltzmann distribution. To ease computational expense in the present study we only have counter ions in the fluid, so the ion number density is simply

$$n(y) = n_o e^{-e\psi(y)/k_B T}, \tag{1.1}$$

where T is the temperature of the fluid (assumed uniform), k_B is the Boltzmann constant, e is the elementary charge (positive), and ψ is the local electric potential which is a function of the wall coordinate y. If we choose the mid-channel potential $\psi(h/2) = 0$, then n_o is the ion concentration at mid-channel. The electric potential in (1.1) satisfies the Poisson-Boltzmann equation

$$\frac{d^2\psi}{dy^2} = -\frac{en(y)}{\varepsilon\varepsilon_o} = -\frac{en_o}{\varepsilon\varepsilon_o} e^{-e\psi(y)/k_B T}, \tag{1.2}$$

where ε_o is the permittivity of a vacuum and ε (assumed constant) parameterizes the dielectric behavior of the fluid. We have assumed monovalent ions. The solution of (1.2)

† Mechanical and Aerospace Engineering, University of California, Los Angeles

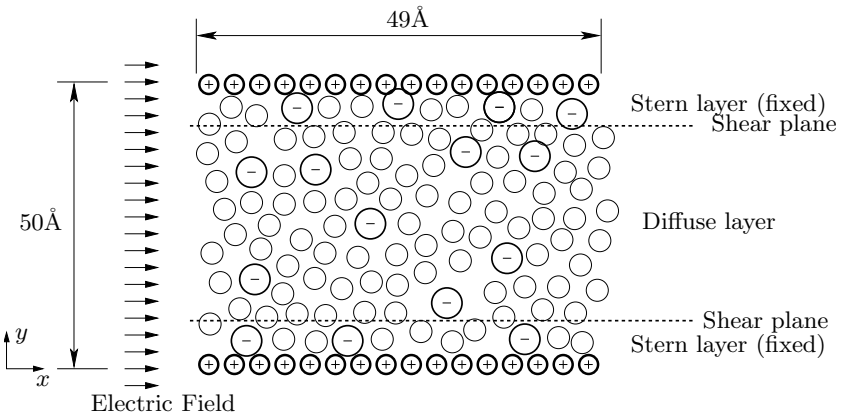

FIGURE 1. Schematic of the electric double layer in a nanometer-scale channel. For simplicity both this schematic and the present simulations only have counter ions in the solution. Two dimensions of the simulated channel are labeled. It also extends 49Å in the z-direction.

is (Israelachvili (1992))

$$\psi(y) = \frac{k_B T}{e} \log(\cos^2 Ky), \tag{1.3}$$

where

$$K^2 = \frac{e^2 n_o}{2\varepsilon\varepsilon_o k_B T}. \tag{1.4}$$

Overall electro-neutrality gives a boundary conditions on ψ in terms of the wall charge density Q_o,

$$Q_o = \varepsilon\varepsilon_o \left.\frac{d\psi}{dy}\right|_{\text{walls}}, \tag{1.5}$$

which can be used to determine n_o. Models have been developed to account for variable permittivity of the medium and variable viscosity (Dukhin & Derjaguin (1974)), but in this initial effort we focus on models that assume constant ε, smooth walls, and infinitesimal ions.

Typically, the ions nearest the wall are assumed to be bound to the surface in the so-called the Stern layer. Beyond the Stern layer is the diffuse layer which is potentially mobile. When there is flow, these two regions are usually assumed to be separated by a shear plane, but since the Stern layer may be only a few atoms thick, it is not clear that this continuum view strictly applies. The dynamics of this near-wall region are important for electro-osmosis, an electrokinetic process by which fluid is drawn through the channel by an applied electric field which exerts a body force on the fluid wherever it has net charge. This process is used to pump fluid in microfluidic devices (*e.g.* Herr *et al.* (2000)) and move fluid through porous material and clays (*e.g.* Coelho *et al.* (1996)). Electro-osmosis is also used in conjunction with theories similar to the one presented above to deduce the ζ-potential, the constant electric potential at the supposed shear plane, so the correctness of these models is also important for making these measurements.

Unfortunately, the small scales involved make it difficult to test electro-osmosis models in detail. For this reason we have developed the capability of simulating the process atomistically. This approach is, of course, limited to channels and pores that are signifi-

Interaction	A (J Å^{12})	C (J Å^6)	ϵ (J)	σ (Å)	r_o (Å)
O-O	4.37×10^{-15}	4.35×10^{-18}	1.08×10^{-21}	3.17	3.55
Cl-O	6.75×10^{-14}	1.03×10^{-17}	3.93×10^{-22}	4.33	4.86
Cl-Cl	1.81×10^{-13}	2.43×10^{-17}	8.16×10^{-22}	4.42	4.96
W-O	5.00×10^{-15}	5.44×10^{-18}	1.48×10^{-21}	3.12	3.50
W-Cl	7.72×10^{-14}	1.29×10^{-17}	5.38×10^{-22}	4.26	4.78

TABLE 1. All parameters for the Lennard-Jones potential. For convenience, two equivalent forms are given: $U(r) = A/r^{12} - C/r^6$ and $U(r) = 4\epsilon(\sigma^{12}/r^{12} - \sigma^6/r^6)$. The final column list r_o, the separation distance corresponding to zero force. All Lennard-Jones potentials were cut off and shifted (Frenkel & Smit (1996)) at the standard $r_c = 2.5\sigma$.

cantly smaller than in present-day manufactured devices, but in many cases the double layers are of nanometer scale and can, therefore, be studied directly by atomistic simulation. This report discusses initial results of this effort. We focus on ion-laden water flow in between idealized surfaces made up of atoms all having the same charge. The interatomic potentials are modeled with established empirical models which are discussed in §2. This section also discusses the numerical methods, the flow parameters, and the simulation procedure. Section 3 presents results for simulated double layers and makes some comparisons with theoretical predictions. A brief summary is provided in §4.

2. Atomistic simulations

2.1. *Physical model*

The waters were modeled using the fixed bond length SPC/E model of Berendsen *et al.* (1987) , which represents hydrogens and oxygens as point charges ($q_H = +0.4258e$ and $q_O = -0.8476$). The oxygens also interact with other atoms by a Lennard-Jones potential. Tests in a nanometer-scale Couette flow showed that the SPC/E model predicted the viscosity of water at $T = 300$K to within 10 percent of the accepted value. The Cl^- were modeled using the parameters of Chandrasekhar *et al.* (1984), and the walls are modeled by fixed square arrays of Lennard-Jones atoms. Parameters for all Lennard-Jones interactions are given in table 1.

2.2. *Numerical method*

A standard velocity Verlet algorithm (Frenkel & Smit (1996)) was used to integrate Newton's equation of motion with a numerical time step of 1fs. Lennard-Jones interactions were computed point-to-point using a cutoff of 2.5σ; Coulomb interactions were computed using an aperiodic implementation (Pollock & Glosli (1996)) of the a P^3M algorithm (Hockney & Eastood (1988)). The mesh for the Poisson solver in the P^3M method had $48 \times 128 \times 48$ points in x, y, and z, respectively, with the same uniform mesh spacing in all three coordinate directions. The 128 mesh points in the y-direction extended over twice the height of the channel and were used to remove the periodicity (Pollock & Glosli (1996)). In our implementation, the point-to-point and mesh portions

of the potential were split using the standard Ewald decomposition,

$$\begin{aligned}\mathbf{F}_i =&\frac{1}{2}\sum_{i\neq j}\frac{q_iq_j}{4\pi\varepsilon_o}\left(-\frac{2\alpha e^{-\alpha^2|\mathbf{x}_{ij}|^2}}{\sqrt{\pi}|\mathbf{x}_{ij}|}-\frac{\mathrm{erfc}(\alpha|\mathbf{x}_{ij}|)}{|\mathbf{x}_{ij}|^2}\right)\frac{\mathbf{x}_{ij}}{|\mathbf{x}_{ij}|}\\ &-\frac{1}{2}\sum_{\mathbf{k}\neq 0}\sum_{j=1}^{N}\frac{q_iq_j}{L^3\kappa^2\varepsilon_o}e^{-\frac{\kappa^2}{4\alpha^2}}i\boldsymbol{\kappa}e^{i\boldsymbol{\kappa}\cdot\mathbf{x}_{ij}},\end{aligned}\tag{2.1}$$

where q_i is the charge and $\mathbf{x}_i$ is the position of the i^{th} atom, and $\boldsymbol{\kappa}$ is a wavenumber vector. The first term in (2.1) was computed using a cutoff of 2.75σ, and the second term was computed on the mesh using fast Fourier transforms. The α parameter, which regulates the relative contributions from the two sums, was set based on numerical experimentation to be $\alpha = 0.262\text{Å}^{-1}$. A matrix constraint method was used to fix the bond lengths of the waters as specified by the SPC/E model.

2.3. *Flow parameters*

The channel dimensions are shown in Fig. 1. The $L_x = L_z = 49$Å dimensions given in the figure are the periodicity lengths of the domain in x and z. The given channel height, $L_y = 50$Å, is measured between the centers of the wall atoms. The wall charge density was $Q_o = 0.24\text{C/m}^2$, which is equivalent to $0.184e$ per wall atom. This high but physically realizable wall charge was selected in this initial study because it gives a relatively large number of counter ions in the fluid and thus provides a good statistical sample within a reasonable computational time. Still, there were only 72 chloride atoms dissolved in the 3,600 waters in the channel. Each wall was constructed from 196 atoms. These charges and numbers are such that the overall system was neutral.

The applied electric field acted on the Cl^- in the x-direction with $F_E = 1.12\times10^{-11}$N. For reference, this is the same force that would be exerted by a point charge 45.3Å away. The energy of this analogous point-charge/point-charge interaction is $12.25k_BT$.

2.4. *Simulation procedure*

To equilibrate the ion distributions, an initial simulation was run with only 2816 atoms, one quarter the eventual number. It was initialized with an approximately uniform distribution of Cl^- and was run for 1 million time steps to obtain a statistically stationary distribution. At this point the domain was doubled in both the x- and z-directions by adding periodic images. When this was done, all atomic positions were perturbed with uniformly distributed random displacements with peak 10^{-3}Å. Because the system is Lyaponov unstable, this small randomization rapidly broke the symmetries. Eight different randomized atomic positions were used as initial conditions for eight separate ensembles that were run simultaneously on different computers to accumulate statistics. For each ensemble, 50,000 time steps were computed to re-equilibrate and allow the different ensembles to develop away from their similar initial conditions. This was followed by 250,000 time steps to gather statistics.

A Berendsen thermostat was used to counter viscous heating and a small temperature drift associated with the P^3M scheme which is accurate but not exactly energy conserving. Velocities were rescaled as

$$\tilde{\mathbf{v}}_i = \chi\mathbf{v}_i\tag{2.2}$$

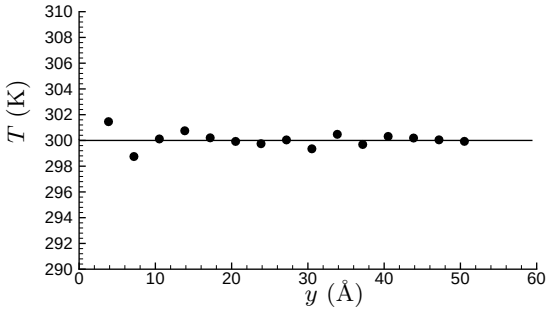

FIGURE 2. Mean temperature. On this and all plots, $y = 0$ corresponds to the centers of the atoms that constitute the low wall.

where

$$\chi = \left[1 - \frac{\Delta t}{\tau}\left(\frac{T_{\rm tar}}{T} - 1\right)\right]^{\frac{1}{2}}, \tag{2.3}$$

and T is the temperature, Δt is the numerical time step (1fs), $T_{\rm tar}$ is the target temperature (300K), and τ is a parameter to regulate the strength of the rescaling. Solutions were shown to be insensitive to the value of τ. The mean scaling factor was nearly unity: $\bar{\chi} = 1 + 4 \times 10^{-7}$. Its greater-than-one value indicates that the numerical energy drift was negative for this flow. Since the instantaneous χ was rarely out of the range $0.9995 < \chi < 1.0005$, it did not alter the dynamics significantly. A difficulty arises in applying thermostats when there is a mean flow because the mean flow must be known *a priori* for its kinetic energy to be distinguishable from thermal kinetic energy. The problem is that the mean is not available until the simulation has run long enough to compute it. Nevertheless, it was found in the present case that results were insensitive to the parabolic flow profile used to estimate the relative contributions, which is no surprise since the mean flow has a peak of approximately 5m/s† and thus constitutes only a tiny fraction of the total kinetic energy of the particles. Ideally, one should remove heat via the walls as in a real channel as done for simple Lennard-Jones fluids by Travis & Gubbins (2000) to avoid any unphysical artifacts associated with the thermostat, but this approach does not provide a rigid control of the temperature in the channel. We also note that (2.2) should technically be applied separately at different distances from the wall because shear and thereby viscous heating is not uniform across the channel. However, application of a single thermostat for the whole channel in the present case resulted in the desired uniform temperature of 300K across the channel as seen in Fig. 2. Pressure was regulated to be one atmosphere by making minor adjustments to the volume of the channel domain.

† In atomistic simulations the time step must be short enough to track the velocities of atoms, which for ordinary temperatures and atomic masses are $\sim 10^3$m/s. Unfortunately, these high atomic velocities make it difficult to converge mean flow statistics when mean flows are typically many times (often several orders of magnitude) smaller than the thermal velocities. Thus seemingly unphysical flow velocities are often used to overcome the signal-to-noise problem. Couette flow tests showed that the SPC/E viscosity was independent of shear rate to considerably higher shear rates than in the present simulations.

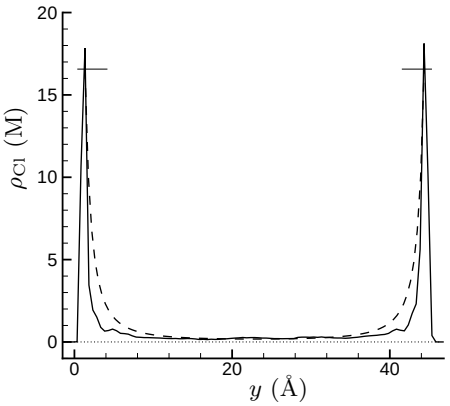

FIGURE 3. Chloride number density: ——— simulation; – – – – (1.1) with ψ from (1.3). The ····· line is $\rho_{\mathrm{Cl}} = 0$. The horizontal line segments demark the peak reached by the – – – – curve.

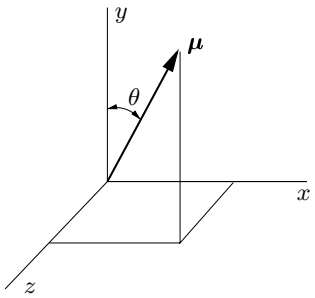

FIGURE 4. Schematic defining θ as the angle that the dipole vector $\boldsymbol{\mu}$ makes with the y-axis.

3. Results

The Cl^- density as a function of distance from the wall is plotted in Fig. 3. As expected, the profile is sharply peaked near the walls and falls to a low value by the middle of the channel. The small bumps near the peak at both walls are believed to result from molecular stacking. They are roughly one water molecule width away from the peak.

The computed profiles differ from the theoretical prediction of (1.1) with $\psi(y)$ from (1.3). The computed profiles have higher peaks at the walls and fall away faster into the channel. A possible explanation for this discrepancy is the finite size of the ions which is neglected in the theory. For example, it is unclear where to apply (1.5) since the precise location of the wall is not well defined. For the theoretical curve in Fig. 3, (1.5) was applied so that the concentration peaks would coincide with those from the simulation, but this is not the closest approach made by the Cl^- in the simulations. Another possible explanation is that the dispersion energy ($U \sim 1/r^6$) is not taken into account in (1.1), but since the Lennard-Jones energy well is deeper (larger ϵ) for the oxygen-wall interaction than for the chloride-wall interaction (see table 1), we expect this to decrease the Cl^- concentration at the wall rather than increase it.

Another possible explanation for the disagreement seen in Fig. 3 is that the dielectric properties of the solvent are altered in the near neighborhood of the charged surfaces. Since the wall is charged, we expect there to be a preferred orientation of the water

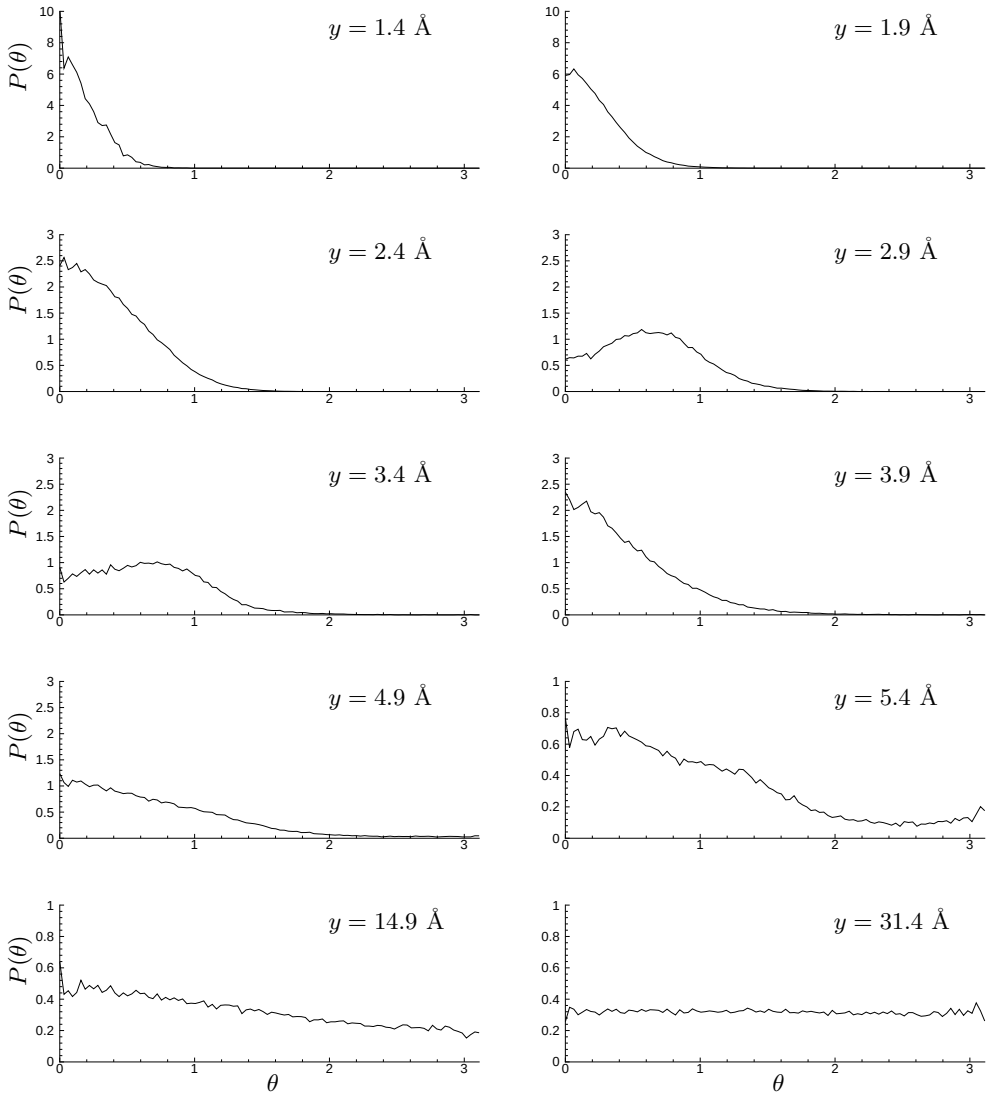

FIGURE 5. Probability density function of water molecule orientations. The angle θ is defined in figure 4. The y-locations correspond to the center of the oxygen atom.

molecules adjacent to it, which will in turn alter their dielectric properties since these waters can not respond to an electric field as they do in bulk. There is experimental evidence for reduced permittivity near a charged surface (Hunter (1981)). With the dipole angle θ defined as in Fig. 4, Fig. 5 shows the probability density (p.d.f.) function of the angular orientation of the waters at different distances from the wall. The p.d.f.'s are weighted so that a random orientation gives a uniform distribution. We see in Fig. 5 that closest to the wall, the dipole vectors are all within 45° of being perpendicular to the wall. Interestingly, the waters at around $y = 3$Å have $\theta \approx 45°$ as their most probable angular orientation, but by $y = 3.9$Å the most probable orientation is again perpendicular to the wall. At larger distance the distribution becomes much more uniform and is nearly flat

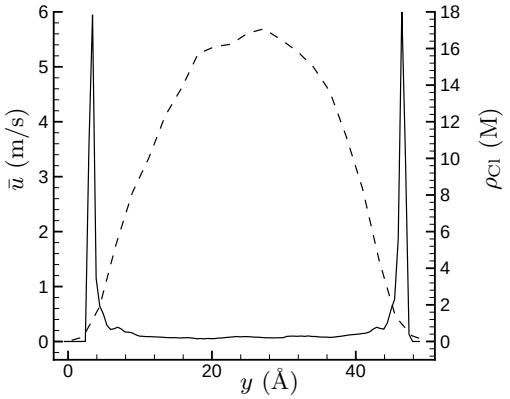

FIGURE 6. The mean flow velocity across the channel - - - - . The mean chloride density is shown on the right axis ——— .

by $y = 15$Å. A preferential orientation would tend to decrease ε and thus increase the apparent strength of the electric field near the wall consistent with Fig. 3.

The computed velocity profile is shown in Fig. 6. We see that it is approximately parabolic in the middle of the channel, but it does not continue as a parabola all the way to the wall. Instead there is considerably more resistance close to the wall. Immediately adjacent the wall the atoms appear fixed in a Stern layer. The details of this are the subject of continuing investigations.

4. Summary

This paper has presented simulations of electro-osmotic flow of an aqueous solution in a 50Å wide channel. It was shown that the ion distribution is in general agreement with a theory that assumes constant permittivity and infinitesimal ions, and it was suggested that non-uniform permittivity due to the preferential orientation of the water molecules in the near-wall region might explain the observed disagreement with this theory. The velocity was found to be approximately parabolic in the middle of the channel, but it flattened out near the walls in the Stern layer. These simulations represent a first step in a continuing effort to identify and model mechanisms in electrically driven nanometer-scale flows.

REFERENCES

BERENDSEN, H. J. C., GRIGERA, J. R. & STRAATSMA, T. P. 1987 The missing term in effective pair potentials. *J. Phys. Chem.* **91**, 6269.

CHANDRASEKHAR, J., SPELLMEYER, D. & JORGENSEN, W. 1984 Energy component analysis for dilute aqueous solutions of Li+, Na+, F-, and Cl- ions. *J. Am. Chem. Soc.* **106**, 903.

COELHO, D., SHAPIRO, M., THOVERT, J.-F. & ADLER, P. 1996 Electro-osmotic phenomena in porous media. *J. Coll. Interf. Sci.* **181**(1), 169-190.

DUKHIN, S. S. & DERJAGUIN, B. V. 1974 *Surface and Colloid Sciences*, volume 7,

chapter Equilibrium double layer and electrokinetic phenomena. John Wiley & Sons, New York.

Frenkel, D. & Smit, B. 1996 *Understanding Molecular Simulation*. Academic Press.

Herr, A. E., Molho, J. I., Santiago, J. G., Mungal, M. G. & Kenny, T. W. 2000 Electroosmotic capillary flow with nonuniform zeta potential. *Anal. Chem.*, **72**, 1053-1057.

Hockney, R. W. & Eastood, J. W. 1988 *Computer simulation using particles*. Institute of Physics Publishing.

Hunter, R. J. 1981 *Zeta potential in colloid science*. Academic Press, London.

Israelachvili, J. 1992 *Intermolecular and Surface Forces*. Academic Press.

Pollock, E. & Glosli, J. 1996 Comments on PPPM, FMM, and the Ewald method for large periodic Coulombic systems. *Comp. Phys. Comm.* **95**, 93-110.

Travis, K. P. & Gubbins, K. E. 2000 Poiseuille flow of Lennard-Jones fluids in narrow slit pores. *J. Chem. Phys.* **112**(4), 1984-1994.